Ultramicroscopy 171 (2016) 19–25

Contents lists available at ScienceDirect

Ultramicroscopy

journal homepage: www.elsevier.com/locate/ultramic

Two-dimensional Kikuchi patterns of Si as measured using an electrostatic analyser

Maarten Vos [a,*], Aimo Winkelmann [b]

[a] Electronic Materials Engineering Department, Research School of Physics and Engineering, The Australian National University, Canberra 2601, Australia
[b] Bruker Nano GmbH, Am Studio 2D, Berlin 12489, Germany

ARTICLE INFO

Article history:
Received 25 May 2016
Received in revised form
12 August 2016
Accepted 18 August 2016
Available online 21 August 2016

Keywords:
Electron backscatter diffraction
Kikuchi
Electrostatic analyser
Silicon
Dynamical electron diffraction theory

ABSTRACT

We present Kikuchi patterns of Si single crystals measured with an electrostatic analyser, where the kinetic energy of the diffracted electron is known with sub-eV precision. Two-dimensional patterns are acquired by rotating the crystal under computer control. This makes detailed comparison of calculated and measured distributions possible with precise knowledge of the energy of the scattered electrons. The case of Si is used to validate the method, and these experiments provide a detailed comparison of measured and calculated Kikuchi patterns. In this way, we can gain more insight on Kikuchi pattern formation in non-energy resolved measurements of conventional electron backscatter diffraction (EBSD) and electron channeling patterns (ECP). It was possible to identify the influence of channeling of the incoming beam on the measured Kikuchi pattern. The effect of energy loss on the Kikuchi pattern was established, and it is demonstrated that, under certain conditions, the channeling features have a different dependence on the energy loss compared to the Kikuchi lines.

1. Introduction

The interaction of energetic electrons with matter is a topic that forms the basis of electron microscopy. For small deflection angles, such as in a transmission electron microscope, the interaction can remain coherent enough to result in observable spot diffraction patterns [1]. For larger scattering angles, the incoherent nature of the interaction wipes out any spot diffraction patterns. Even in that case, however, coherent diffraction still has to be considered for the incoming and outgoing trajectories before and after the incoherent scattering event, respectively. Coherent small-angle deflections of the incident electron beam result in diffraction effects often called “electron channeling” [2], and exactly the same type of effects lead to Kikuchi band formation along the outgoing directions [3]. In both cases, the term “channeling” is best understood as the perceptible operation of electron diffraction effects on the backscattered electron signal, which will be most pronounced near possible Bragg reflection conditions.

Kikuchi band formation is a physical key process of EBSD (Electron Backscatter Diffraction), a tool that is widely used to determine the orientation of the different grains in polycrystalline samples [4]. A detailed interpretation of Kikuchi patterns is possible by comparing them to calculated patterns based on the dynamical theory of diffraction [5]. In EBSD, a phosphor screen is used to measure the Kikuchi pattern. This method is straightforward, simple to set up, and very efficient, but the observed pattern is the consequence of electrons with a broad and generally poorly known distribution of energies hitting the phosphor screen. The backscattered energy distribution extends from the incoming beam energy essentially all the way down to zero, but the diffraction effects are presumed to be concentrated near the incident beam energy. This is why, for reasons of efficiency, theoretical simulations can approximately assume an effective fixed energy for the Kikuchi diffraction effects. It is not exactly known, however, in which way the value of this effective beam energy is determined for arbitrary materials [6].

For a thorough test of our understanding of the transport of electrons in matter it is thus important to measure the Kikuchi patterns for the case of well-defined outgoing energies. A step towards this goal was made by Deal et al. [7], who used a retarding field analyser as a high-pass filter to transmit only electrons exceeding a certain energy. Indeed, the diffraction pattern obtained showed more structure if the range of energies of electrons hitting the phosphor screen was limited to energies near that of the incident beam.

Even better (sub-eV) energy resolution can be obtained using electrostatic analysers [8]. Then it is possible to differentiate the Kikuchi pattern caused by electrons scattered from light and heavy atoms in a compound as, due to the recoil effect, their kinetic energy is slightly different [9]. Due to experimental limitations of

* Corresponding author.
E-mail address: maarten.vos@anu.edu.au (M. Vos).

http://dx.doi.org/10.1016/j.ultramic.2016.08.015
0304-3991/

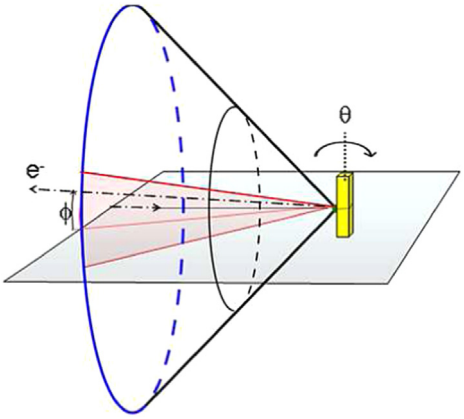

Fig. 1. Schematic of the experiment. The spectrometer measures electrons that move along a range of azimuthal directions ϕ which are on the surface of a cone of constant scattering angle. The incident beam is along the central axis of this cone. The measurement is repeated for different values of the sample rotation θ, changing the incidence angle on the surface. In this way a two-dimensional (θ, ϕ) distribution is obtained. For the detailed experimental setup related to energy-resolved diffraction effects, see [8].

the spectrometer, the intensity distribution in these previous studies was only obtained along 1d lines of outgoing directions, rather than in true 2d-patterns.

Here we describe experiments that overcome this limitation. The rotation of the sample was automated and a two-dimensional pattern was obtained from a set of line distributions, all acquired for the same amount of accumulated charge, but for slightly different sample orientations. This makes it possible to compare the calculated 2d-Kikuchi pattern, based on a specific energy, with the one obtained experimentally for that energy.

2. Experimental details

The experimental set-up is sketched in Fig. 1. An electron beam with 40 keV (0.2 mm diameter) impinges on the sample. The detector measures electrons emerging (within 0.1°) along a segment of the surface of a cone with half cone angle of 44.3°. The measured segment is $\Delta\phi \approx 11°$ out of 360° of the total cone. The incoming beam is along the axis of this cone. All electrons have thus scattered over 135.7°. The sample is mounted on a precision rotary feedthrough which can be rotated by a stepper motor under computer control.

Beam current is measured (around 10 nA) and the collected charge is integrated during the measurement. Data are acquired at each angle for a preset amount of charge. The electron analyser, consisting of a set of slit lenses followed by a hemispherical analyser, has a two-dimensional detector that measures the ϕ range and energy window of 40 eV simultaneously, and counts individual electrons hitting the detector. The energy resolution of the system is about 0.4 eV, the angular resolution in θ and ϕ is about 0.1° [10]. The intensity of the spectrum at each ϕ angle is determined for different user-defined energy loss ranges. When the pre-set amount of charge was collected the θ angle was incremented and the measurement was repeated. Unless otherwise stated the θ-step size was 0.1°. A measurement sequence at 100 different θ angles took about 24 h.

The Si crystals were sputtered with 2 keV Ar^+ ions and annealed at ≈600° before the measurement. The orientation of the crystal was judged from the cleavage planes and the exact orientation was found by matching the observed intensity

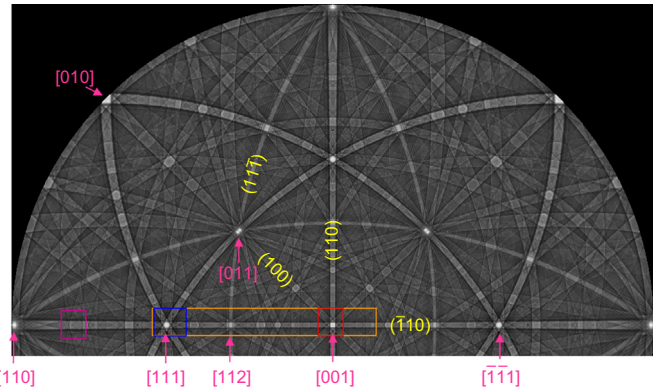

Fig. 2. Stereographic projection of calculated Kikuchi bands in silicon at 40 keV. Main planes and directions are indicated. The approximate areas measured with the electrostatic analyser are indicated by boxes. (For interpretation of the references to colour in this figure caption, the reader is referred to the web version of this paper.)

distribution to the calculated one.

For these measurement conditions (scattering angle ≈135°, energy 40 keV) the recoil energy transferred to the target atoms in the large-angle deflection is well resolved. In some cases we evaporated 2 Å Au on the surface. This gave a well-resolved Au peak in the backscattered electron spectrum, with an intensity that is not expected to depend on the ϕ angle. Thus the Au peak could be used to determine the channel plate efficiency variations. In reality, as we will see, the Au affected the Kikuchi pattern somewhat. Therefore the channel plate response was measured independently of the actual single crystal measurements.

3. Theory

The Kikuchi patterns of silicon were simulated using the Bloch wave approach of dynamical electron diffraction theory [5] as implemented in the software *ESPRIT DynamicS* (Bruker Nano, Berlin). We took into account a total of 1758 reflectors *hkl* with a maximum reciprocal lattice vector length of $1/d_{hkl} < (1/0.035)\text{nm}^{-1}$ and a relative strength of larger than 7% of the strongest reflector intensity (square of the absolute value of the structure factor). A mean square displacement of 0.00015 nm^2 was used to consider thermal vibrations of the crystal structure via the Debye–Waller factor. As inelastic mean free path a distance of 20 nm was assumed. The obtained Kikuchi pattern is shown in Fig. 2.

4. Results

4.1. Zone axis Kikuchi patterns

The Si crystal with a [0 0 1] surface normal was mounted such that the (1 1 0) plane was approximately horizontal. For each θ value the (1 1 0) plane was within the field of view of the analyser and this Kikuchi band was thus always observed. By rotating the crystal in such a way that the surface normal is pointed towards the analyser one can measure the Kikuchi patterns near the [0 0 1] direction. The results are shown in the top panel of Fig. 3. The area measured corresponds to the red box in Fig. 2. The experimental spectrum shows a strong peak, when the [0 0 1] points towards the analyser and this direction defines $\theta = 0$, $\phi = 0$. In the lower half of Fig. 3 we show the corresponding theoretical result. In both experimental and theoretical plot the bottom plane correspond to zero intensity. Agreement between simulation and experiment is striking, most of the intricate features shown in the calculations

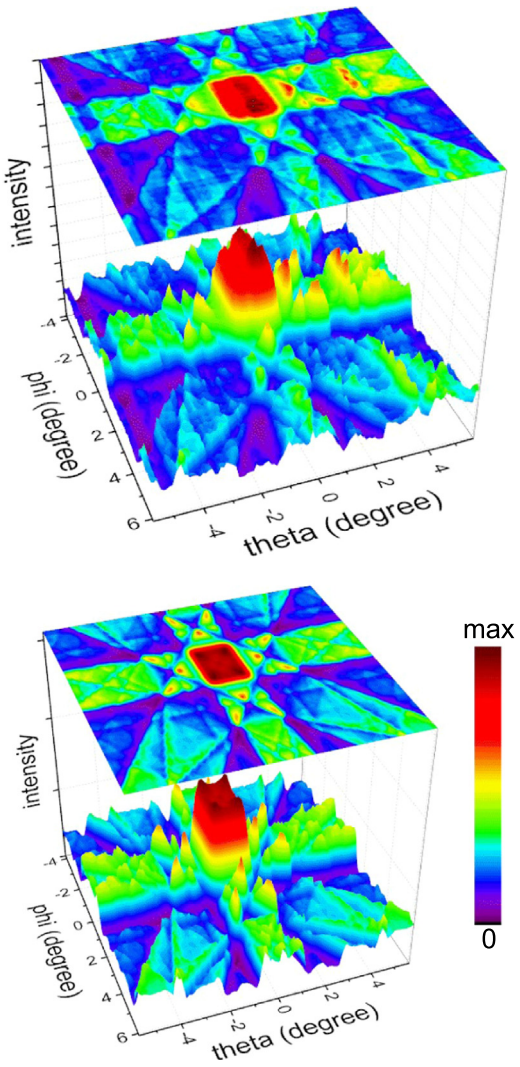

Fig. 3. Measured (top) and calculated (bottom) Kikuchi intensity distribution near the [1 0 0] direction.

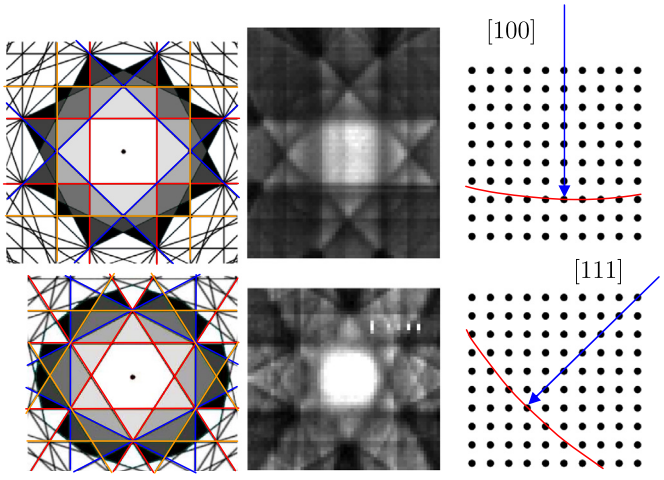

Fig. 4. The measured intensity distributions near the [0 0 1] and [1 1 1] directions (center) compared to the corresponding two-dimensional Brillouin zones and Bragg planes (left). The right panel illustrates that, when the beam is along a symmetry direction, the shortest reciprocal lattice vectors on the Ewald sphere are all in the same plane.

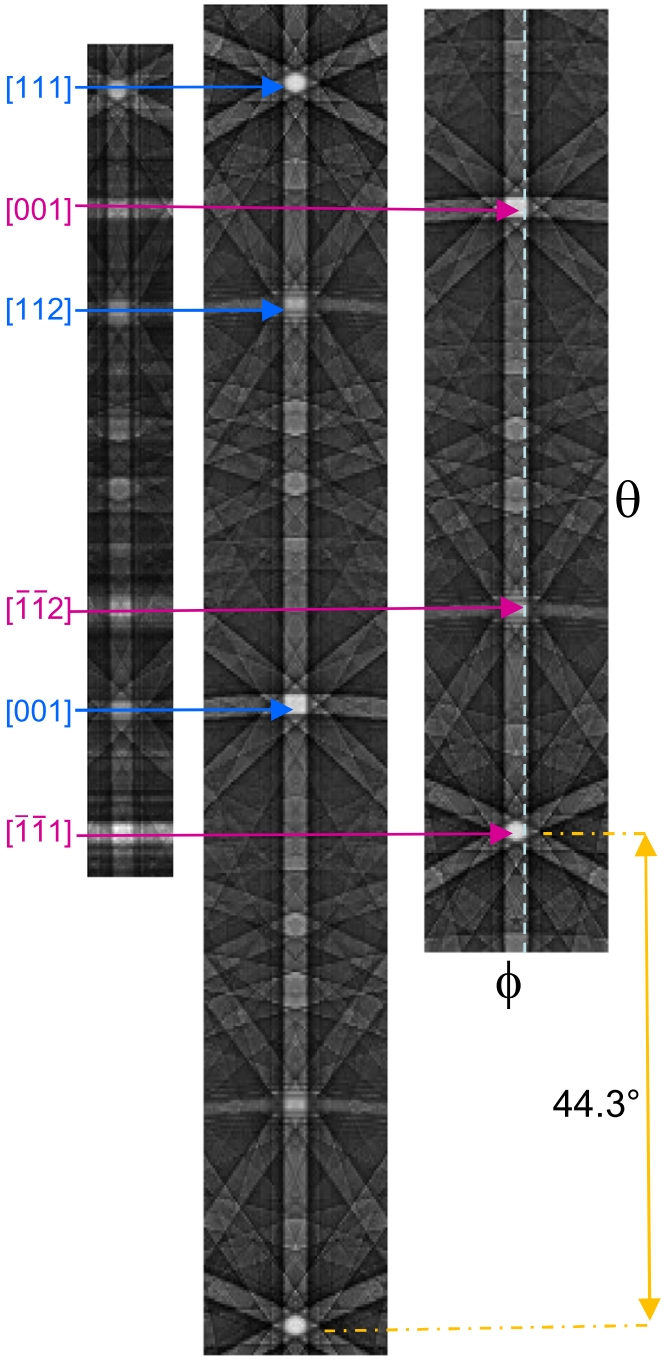

Fig. 5. Experimental Kikuchi pattern intensity distribution, as measured over a large θ range (left) compared to the theoretical result for outgoing diffraction effects (middle), and the simulation for the ingoing diffraction (right). In our experimental setup (Fig. 1) the incident beam direction is rotated by 44.3° with respect to the outgoing direction at $\phi = 0°$. The electron beam thus samples a correspondingly incident direction shifted in the figure along the vertical (0 1 0) band. Whenever the incident beam is near a zone axis of the vertical band, the complete intensity at all scattering cone angles ϕ is intensified. The vertical dashed line in the right panel is a *possible* set of directions probed by the incoming beam, but the precise alignment of this line is unknown.

are reproduced in the experiment.

There are also clear differences. For example, the experiment shows at $\theta = 4°$ a line of enhanced intensity, not seen in the simulation. Around $\theta = -5°$ there is a band of reduced intensity in the experiment, also absent in the calculations. These features are

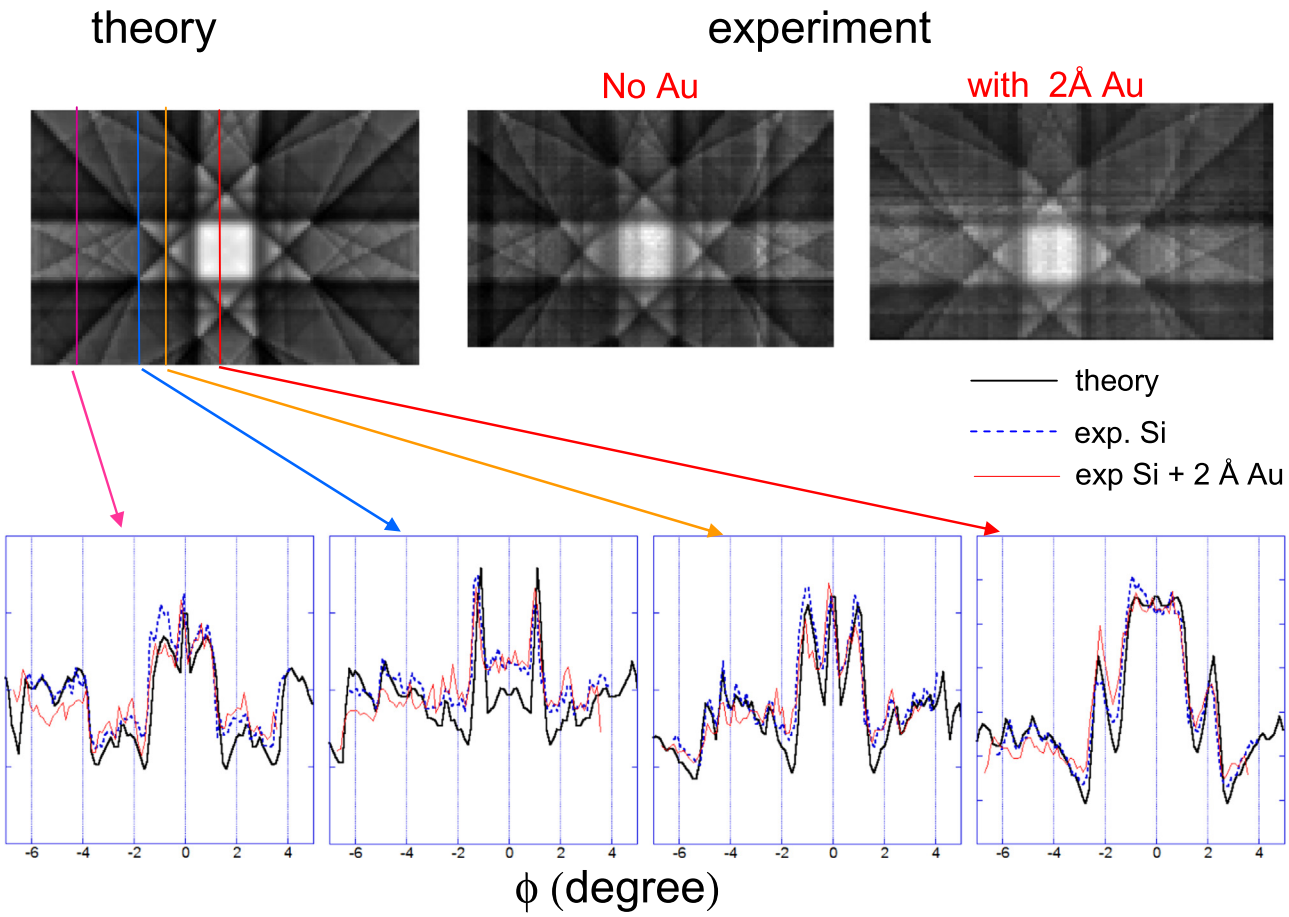

Fig. 6. The calculated and measured (with and without Au at the surface) intensity distribution for Si near the [1 0 0] direction.

not symmetrical with respect to $\theta = 0$. We interpret these as channeling effects of the incoming beam, modifying the probability of large-angle deflection into the analyser.

As is well known, the geometrical structure of the zone axis Kikuchi patterns can be understood as resulting from corresponding structure in reciprocal space. In this context, the relation between the Kikuchi lines, Bragg planes and Brillouin zones is relevant, see e.g [11] for an extensive discussion. For high energies, the Ewald sphere is quite flat, and near symmetry directions the Ewald sphere intersects nearly with the reciprocal lattice points in the plane perpendicular to the symmetry direction (zero order Laue zone, ZOLZ) [1]. The resulting Kikuchi pattern resembles the 2d-Brillouin zones, as on the Brillouin zone boundary the diffraction condition $2\boldsymbol{k}_0 \cdot \boldsymbol{g} + g^2 = 0$ is fulfilled. This is illustrated in Fig. 4. The Brillouin zone boundaries corresponding to the 3 shortest reciprocal lattice vectors are reproduced in colour. These Bragg planes are all easily observed in the experimental pattern. The contribution of higher order planes are generally too small to be identified unambiguously.

The two-dimensional approach has limitations, even near the zone axis directions. It would predict a 6-fold symmetry axis for the $[\bar{1}\,\bar{1}\,1]$ direction. In reality, the pattern has only a three-fold symmetry axis. Deviations from 6-fold symmetry are indicated by the yellow arrows in Fig. 7 (to be discussed later) in both the calculated and measured intensity distribution. These arrows point to darker triangles. that are not seen when the pattern is rotated by 60°. Thus diffraction vectors outside the two-dimensional plane play a role as well (higher order Laue zones, HOLZ [1]).

4.2. Incident beam diffraction effects

To further analyze the effect of channeling of the incoming beam we did a long scan (with larger step size: $\Delta\theta = 0.25°$) extending from the [1 1 1] direction past the [0 0 1] direction (Fig. 5). The measured area corresponds approximately to the orange box in Fig. 2. The high-symmetry directions are easily identified in the result, and when plotted next to the theoretical results it is clear that many of the minor details are reproduced by the experiment as well. Deviations are visible in the form of horizontal bands in the experiment, not seen in the simulation. These horizontal bands are again attributed to channeling of the incoming beam. The incoming beam, the centre of the slit lens of the analyser, and the surface normal are all approximately in the same plane. If an outgoing direction points towards the centre of the analyser at $x°$ it will point towards the gun at $(x + 44.3)°$. The same physics governs the directional effects for the incoming and outgoing electrons. Thus we can identify the main channeling directions of the incoming beam by shifting the theoretical result by 44.3°, as is done in the right panel of Fig. 5. Indeed the major enhancements seen in the experiment, not seen in the simulation for the outgoing trajectories, coincide nicely with the incoming beam being close to the [0 0 1], $[\bar{1}\,\bar{1}\,2]$ and $[\bar{1}\,\bar{1}\,1]$ directions.

In Fig. 5, we observed that the backscattered intensity carries diffraction effects that depend on the outgoing angle ϕ ("channeling-out"). This ϕ-dependent structure as a whole is multiplied by a factor that carries diffraction effects depending only on the incident beam direction angle θ ("channeling-in"). Concerning the theoretical description, the overall modulation of the

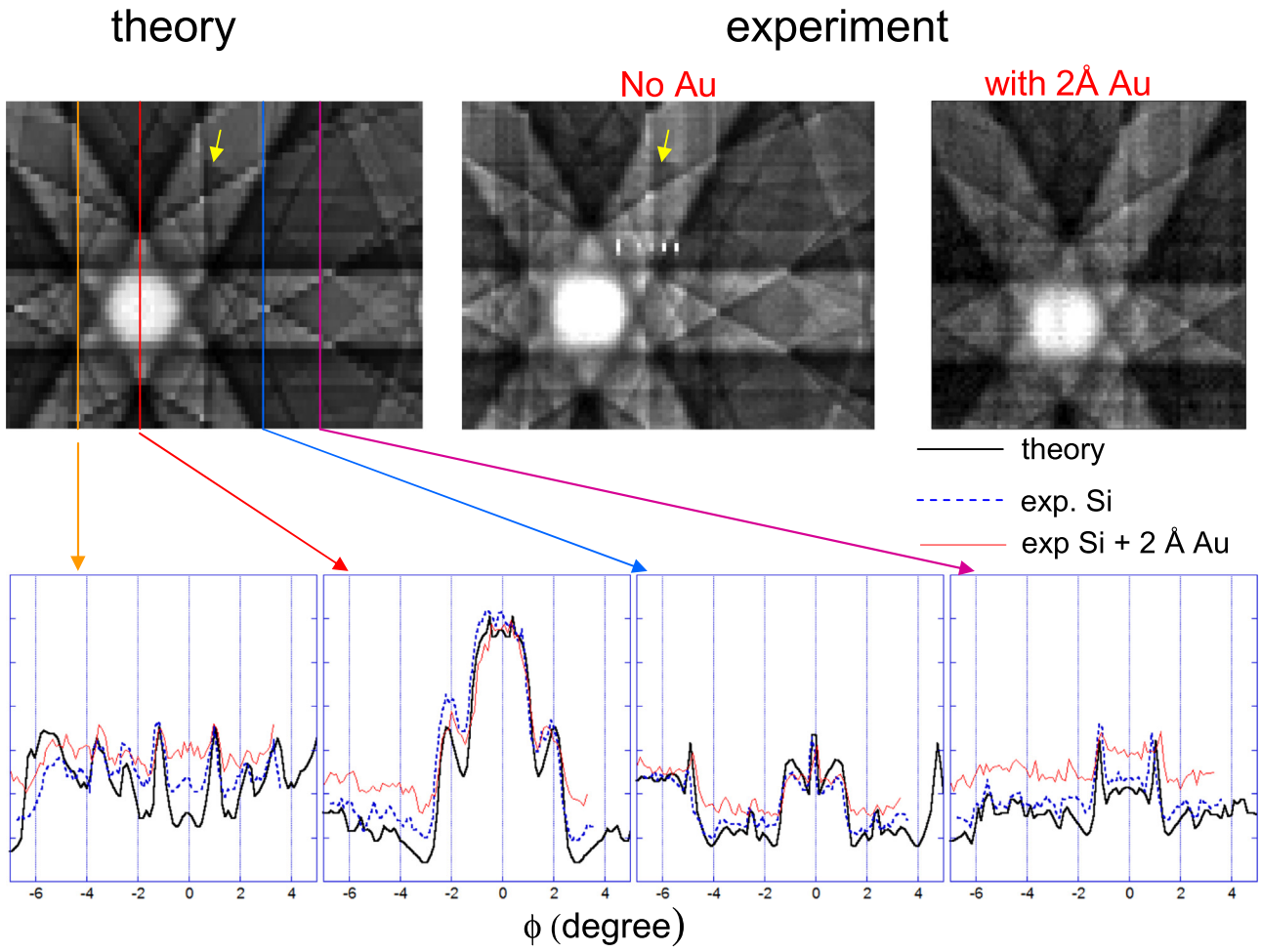

Fig. 7. The calculated and measured (with and without Au at the surface) intensity distribution for Si near the [1 1 1] direction.

backscattered intensity I_{BSE} is thus given by the product of two terms $I_{in}(\theta) \times I_{out}(\theta_{out}, \phi_{out})$. The first term, $I_{in}(\theta_{in})$, describes the intensity that is created at each backscattering atom and which varies as a function of the incident angle θ_{in} due to diffraction effects along the incident wave vector (in the setup used here, ϕ_{in} is fixed). The second factor, $I_{out}(\theta_{out}, \phi_{out})$, describes the variation of intensity due to diffraction in the outgoing path for an atomic source of unit strength. In our previous investigation [9] we showed unambiguously that Kikuchi pattern formation is intrinsically linked to a measurable recoil energy loss that is required by the momentum transfer to an individual atom (in contrast, coherent electron reflection transfers only an infinitesimal energy to an extended crystalline region containing many atoms).

In an important analysis of the relationship between different diffraction effects in the SEM, Wells in [12] argued for the "channeling in and channeling out" model that seemed to be in conflict to a two-event "diffraction model" (diffuse scattering followed by diffraction) for the formation of electron backscattering patterns. Our previous results in [9] in combination with Fig. 5 allow us to conclude that the contradiction assumed in [12] is only an apparent one in the sense that "channeling in" and "channeling out" are nothing else than diffraction effects and the "diffuse scattering" is the incoherent recoil scattering. The "channeling in and channeling-out" – model of electron diffraction effects in the SEM [12] could thus be more specifically named the "channeling in – recoil – channeling out" ("CIRCO") – model.

4.3. Influence of Au deposition

Deposition of additional materials onto a crystalline surface can be used, for example, to study details of EBSD pattern formation [13], or to alleviate problems of sample charging in EBSD studies from non-conductive materials [14]. The deposition of amorphous material will tend to reduce the observed diffraction contrast, and also any possible modifications of the near-surface crystal structure need to be considered.

The energy-resolved detection in our experiment enables us to study the influence of the deposition of small amounts of Au in a more detailed way than by conventional EBSD measurements. Moreover, a comparison to theoretical calculations which assume perfect crystals will make it possible to study the influence of such surface modifications on the agreement between simulations and experiments.

Quantitative comparisons are made in Figs. 6 and 7 for the detailed scans near the $[1\,1\,1]$ and $[0\,0\,1]$ direction (blue and red box in Fig. 2). Measurements were done for Si with and without 2 Å of Au deposited on its surface. For the $[0\,0\,1]$ direction the influence of Au was rather minor, but it caused a significant reduction in contrast near the [1 1 1] direction. Au is known to react with the Si crystal see e.g. Ref. [15], and the thickness of the surface layer disturbed by the Au could be considerable thicker than

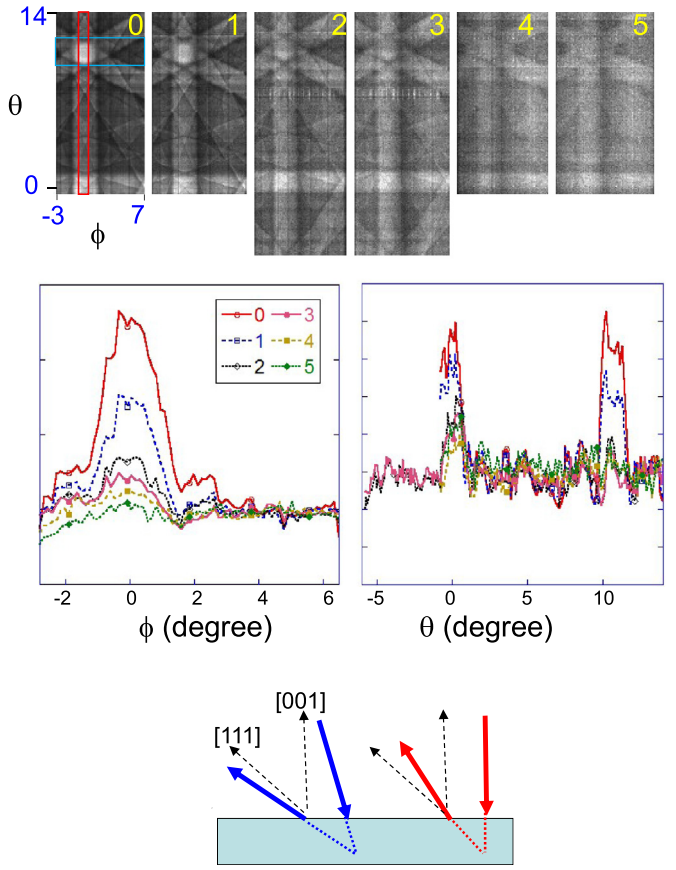

Fig. 8. Kikuchi contrast as a function of the energy loss of the detected electrons. The energy loss corresponds to the elastic peak or the creation of 1–5 plasmons as indicated. The angular distribution shown in the middle-left panel corresponds to the intensity in the blue box shown in the grey-scale image of the zero plasmon case (integrated over θ), the distribution in the centre right panel corresponds to the red box (integrated over ϕ). The lower panel shows the measurement geometry at the top (blue) and bottom (red) end of the scan relative to the crystallographic directions. The θ coordinate refers to the angle of the incoming beam with the [0 0 1] surface normal. (For interpretation of the references to colour in this figure caption, the reader is referred to the web version of this paper.)

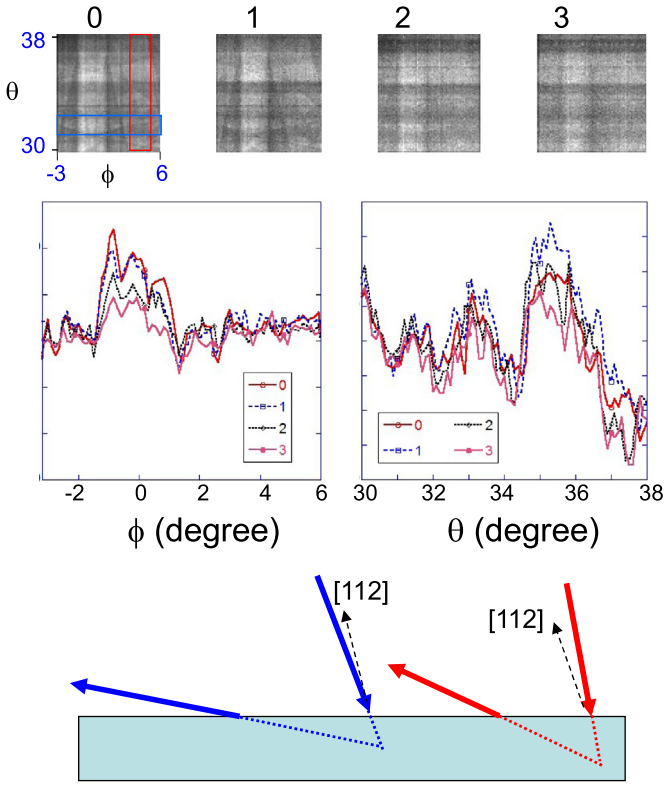

Fig. 9. Measurement of Kikuchi patterns at energy losses corresponding to the number of plasmons, as indicated for a glancing out geometry. The length of the outgoing trajectory part is about 3–5 times larger than the ingoing one. The contrast of the Kikuchi pattern (center-left panel obtained by integrating the intensity in the blue rectangle over θ) reduces quickly with energy loss but the horizontal banding resulting from channeling effects (as seen in the center-right panel obtained by integrating the intensity in the red rectangle over ϕ) for the incoming beam is almost independent of the energy loss. The relative intensity of the features should be compared to the overlapping region of the blue and red regions, which here are assumed to be less influenced by ingoing or outgoing diffraction effects. (For interpretation of the references to colour in this figure caption, the reader is referred to the web version of this paper.)

2 Å. For the [1 1 1] direction the path length through the disturbed layer is longer than for the perpendicular [0 0 1] direction. This could explain, at least in part, why one direction is more affected by the Au layer than the other direction.

4.4. Role of inelastic scattering

So far we have used the elastic peak to construct the diffraction patterns. No electronic excitations were created by the electrons that contribute to the elastic peak. The average total (incoming plus outgoing) path length of the corresponding no-loss trajectories is the inelastic mean free path. By tuning the energy of the detected electrons away from the elastic peak, one can investigate the contrast in the diffraction patterns after inelastic losses. The corresponding paths will be, on average, longer. This is illustrated in Fig. 8 for outgoing directions near [1 1 1]. The measured angular ranges of the experiments shown in Fig. 8 include the direction where the surface normal direction [0 0 1] coincides with the incoming beam, resulting in strong channeling of the incoming beam. The 10° angular separation of the two main features is consistent with the scattering geometry of our setup (opening angle of the scattering cone of 44.3°) and the crystallography of the cubic Si lattice (the angle between [0 0 1] and [1 1 1] is 54.7°). The energy losses selected corresponds to an energy window of 3 eV wide centered at the elastic peak and at 17, 34, 51, 68 and 85 eV away from this peak corresponding to the creation of 0 to 5 plasmons, respectively. With increasing number of plasmons created, a lot of the detailed information in the Kikuchi pattern disappears. For distributions obtained at an energy loss corresponding to the creation of 5 plasmons only a hint remains of the major bands, and all detail has disappeared. Similar conclusions were reached before based on measurements of the Kikuchi bands along single lines [8]. Note that at $\theta = 0°$, the horizontal [001] channeling feature for the incoming beam also reduces intensity with increasing losses, however, apparently with a less severe reduction in dependence on the number of plasmon losses, as can be seen in line plots the middle right panel of Fig. 8. The intensity of the [0 0 1] channeling-in feature at $\theta = 0°$ reduces more slowly with the number of plasmon losses than the channeling-out feature of the [111] zone axis at $\theta = 10°$. This observation also supports the interpretation that a given number of plasmon losses is less likely to occur on the shorter incoming path.

In the experiment shown in Fig. 8 the incoming and outgoing trajectories are of rather similar length. For the incoming beam at θ and our experimentally fixed scattering angle $\theta_S = 44.3°$, the length l_i of the incoming trajectory with elastic backscattering at depth t_S below the surface is $l_i = t_S/\cos(\theta)$, while the corresponding outgoing part l_o of the trajectory is $l_o = t_S/\cos(\theta + \theta_S)$. For the ratio

l_o/l_i we thus have $l_o/l_i = \cos(\theta)/\cos(\theta + \theta_S)$, with θ measured positively for angles like shown in Fig. 8.

While in Fig. 8 we had approximately $l_o/l_i = 1/\cos(45) = 1.4$, we now show in Fig. 9 data that was taken for the sample rotated to a position where the length of the outgoing trajectory is much longer than the ingoing length. The outgoing directions of this measurement correspond to the pink box in Fig. 2, and are rather glancing with the ingoing θ near 35°. For the outgoing-to-ingoing ratio near these angles we have $l_o/l_i = \cos(35)/\cos(45 + 35) = 4.7$ There are no major zone axes in this region but the $(1\,1\,1)$ plane and minor planes are well visible for the zero energy loss case. The $(1\,1\,1)$ band gets fainter and the minor features disappear with increasing energy loss, that mainly occurs along the longer outgoing trajectory. These measurements contain the direction where the [1 1 2] direction is along the incoming beam. The channeling along the incoming beam causes the broad horizontal band in the distribution. In the incoming channeling data shown in right middle panel of Fig. 9 it is striking that the incoming channeling feature near 35° is quite weak for elastic scattering and then actually becomes stronger at the first plasmon loss. For zero energy loss, the trajectory lengths are small, with the incoming trajectories approximately from 3 up to 5 times shorter than the outgoing ones in our case. For very small path lengths, less than approximately one extinction distance [1], the dynamical diffraction effects are generally less pronounced, which reduces the internal modulation of the standing Bloch wave field in the crystal which is sensed by the backscattering event. Experimentally, we fix the number of plasmon losses, which will happen more often on the outgoing path than in the incoming due to the geometry chosen. A trajectory with plasmon loss is in total longer than an elastic trajectory, thus also the incoming path will be longer on average. This can increase the diffraction contrast due to the incoming beam because more material is involved, while the probability of plasmon loss is low compared to the outgoing path. With increasing number of losses, the dynamical diffraction effects will fully develop and saturate and the reduction of contrast due to the plasmon losses in the incoming path will start to dominate. In the experimental data, we see that at larger energy loss the band due to incoming channeling actually becomes the stronger feature. A similar effect has been discussed in [8] for the reciprocal geometry with ingoing and outgoing path reversed. There it was shown that highest *outgoing* diffraction contrast can be observed not at the elastic peak but instead for energy losses of a few plasmons (in a geometry that has a long ingoing trajectory as compared to a relatively short outgoing trajectory).

It is important in the interpretation of these measurements that the quasi-elastic backscattering event separating incoming and outgoing trajectories is located at an atomic position and not anywhere in the unit cell [16]. This has a decisive effect on the different implications of inelastic processes in the outgoing as compared to the incoming path when they have very different relative lengths. The backscattering event relocates any inelastically scattered electron to a specific position in the unit cell, which is a precondition for diffraction patterns to be observed [16].

This observation illustrates how the two-dimensional energy-resolved measurements make it possible to clearly differentiate between diffraction effects along the incoming and along the outgoing trajectory.

5. Conclusion

We demonstrated that it is possible to obtain highly detailed 2-dimensional distributions of the intensity of scattered electrons from a single crystal using an electrostatic analyser with sub-eV resolution. In the case of Si diffraction along the incoming beam and along outgoing trajectories were identified. The dependence on the diffraction contrast was studied as a function of the energy loss. It was demonstrated that in certain cases the influence of the energy loss on diffraction differs for the incoming and outgoing beam. It was also shown that a Au surface layer of several Å thick can reduce the contrast. As Au is known to react with Si, the extension of the distortion of the lattice can exceed the nominal Au thickness. The influence of overlayers (either epitaxial or random) on the Kikuchi contrast of both the substrate and overlayer atoms (assuming that these contributions can be separated by the recoil effect) could provide a new window on overlayer growth, able to probe more thicker overlayers and measure smaller strains than possible with photo-emission. Here there could be many more interesting research opportunities.

In short these experiments can be used to increase our insight in Kikuchi pattern formation, help clarify the physics involved and could open new ways of studying overlayer growth. More generally it is a good way of testing the accuracy of numerical implementations of the dynamical theory of diffraction.

Acknowledgements

This work was made possible by a grant of the Australian Research Council.

References

[1] D.B. Williams, C.B. Carter, Transmission Electron Microscopy, 2nd ed., Springer Science + Business Media, New York, 2009.
[2] D.C. Joy, D. Newbury, D. Davidson, J. Appl. Phys. 53 (1982) R81.
[3] M.N. Alam, M. Blackman, D.W. Pashley, Proc. R. Soc. A: Math. Phys. Eng. Sci. 221 (1954) 224.
[4] A.J. Schwartz, M. Kumar, B.L. Adams, D.P. Field (Eds.), Electron Backscatter Diffraction in Materials Science, Springer, 2009.
[5] A. Winkelmann, C. Trager-Cowan, F. Sweeney, A.P. Day, P. Parbrook, Ultramicroscopy 107 (2007) 414.
[6] A. Winkelmann, in: A.J. Schwartz, M. Kumar, B.L. Adams, D.P. Field (Eds.), Electron Backscatter Diffraction in Materials Science, Springer, Berlin, 2009 (Chapter 2).
[7] A. Deal, T. Hooghan, A. Eades, Ultramicroscopy 108 (2008) 116.
[8] A. Winkelmann, K. Aizel, M. Vos, New J. Phys. 12 (2010) 053001.
[9] A. Winkelmann, M. Vos, Phys. Rev. Lett. 106 (2011) 085503.
[10] M. Vos, G.P. Cornish, E. Weigold, Rev. Sci. Instrum. 71 (2000) 3831.
[11] M. Gajdardziska-Josifovska, J.M. Cowley, Acta Crystallogr. Sect. A 47 (1991) 74.
[12] O.C. Wells, Scanning 21 (1999) 368.
[13] S. Zaefferer, Ultramicroscopy 107 (2007) 254.
[14] J.K. Farrer, J.R. Michael, C.B. Carter, EBSD of Ceramic Materials, in: Electron backscatter diffraction in materials science, first ed., Springer, New York, 2000, pp. 299–318.
[15] L. Braicovich, C.M. Garner, P.R. Skeath, C.Y. Su, P.W. Chye, I. Lindau, W.E. Spicer, Phys. Rev. B 20 (1979) 5131.
[16] A. Winkelmann, M. Vos, Ultramicroscopy 125 (2013) 66.